

# On the observed duration distribution of gamma-ray bursts from collapsars

D. Lazzati<sup>1</sup>, M. Villeneuve<sup>2</sup>, D. López-Cámara<sup>1</sup>, B. J. Morsony<sup>3</sup>, and R. Perna<sup>2,4</sup>

<sup>1</sup>*Department of Physics, NC State University, 2401 Stinson Drive, Raleigh, NC 27695-8202*

<sup>2</sup>*Department of Astrophysical and Planetary Sciences, University of Colorado, Boulder, CO 80309-0391, USA*

<sup>3</sup>*Department of Astronomy, University of Wisconsin-Madison, 3321 Sterling Hall, 475 N. Charter Street, Madison WI 53706-1582*

<sup>4</sup>*JILA, University of Colorado and National Institute of Standards and Technology, Boulder, CO 80309-0440, USA*

21 October 2018

## ABSTRACT

The duration of the prompt emission of long gamma-ray bursts is generally considered to be fairly similar to the duration of the activity of the engine in the center of the progenitor star. Here, we investigate the relation between the duration of the engine activity and that of the observed light curve, using inputs from both numerical simulations and observations. We find that the observed burst duration is a good proxy for the engine duration after the time necessary for the jet to break out the star’s surface is subtracted. However, the observed duration is a function of the viewing angle and can be significantly shorter than the duration of the engine activity. We also show that the observed, redshift-corrected burst duration evolves only moderately with redshift for both observations and synthetic light curves. We conclude that the broad distribution of the observed duration of long BATSE gamma-ray bursts is mostly accounted for by an engine lasting  $\sim 20$  s, the dispersion being due to viewing and redshift effects. Our results do not rule out the existence of engines with very long duration. However, we find that they are constrained to be a small minority of the BATSE detected bursts.

**Key words:** gamma-rays: bursts — hydrodynamics — methods: numerical — relativity

## 1 INTRODUCTION

Gamma-ray bursts (GRBs), the most energetic explosive phenomena known today, have historically been classified based on the time during which 90% of their flux is observed ( $T_{90}$ ). Since the early epoch of the BATSE observations, it became apparent that the distribution of durations is bimodal, with a clear minimum that, depending on the sensitivity of the instrument, lies between 1 and 3 seconds (Kouveliotou et al. 1993; see also Nakar 2007). Bursts with durations between milliseconds to about 2 seconds are classified as “short” (SGRBs), while the class of “long” GRBs (LGRBs) is characterized by a  $T_{90}$  of more than 2 seconds, and the observed distribution extends up to a few hundred seconds.

Based on the duration distribution and difference in the hardness ratio, it was theorized that the progenitors of these bursts are of different origin (Kouveliotou et al. 1993). SGRBs are now believed to be associated with the merger of two compact objects (Nakar 2007), while LGRBs are thought to be associated with the collapse of massive stars (Woosley & Bloom 2006). Even though alternative classification schemes have been attempted (Gherels et al. 2006;

Zhang et al. 2007; Kann et al. 2011), the duration of a burst is critical to the progenitor type. Throughout the rest of this paper we will focus on LGRBs.

Collapsars are Type Ibc core-collapse supernovae formed from massive Wolf-Rayet stars that are rotating very fast and produce jets of relativistic matter along their rotation axes (MacFadyen & Woosley 1999, Nagataki 2011). The core of these progenitors evolves to become a black hole, which accretes at super-Eddington rates from a disk formed from the fallback material<sup>1</sup>. For a typical star, the jet takes about 10 s to cross the star and break out on the surface (MacFadyen & Woosley 1999; Aloy et al. 2000; Zhang et al. 2003; Morsony et al. 2007; Bromberg et al. 2011, 2013; López-Cámara et al. 2013). This means that, for GRBs with observed durations of  $\sim 2$  s, the engine must be active just a little longer than the

<sup>1</sup> An alternative model is the magnetar model in which the core evolves to a fastly spinning, highly magnetized neutron star (e.g. Usov 1992; Bucciantini et al. 2009). Since our jets are injected as boundary conditions, the true nature of the central engine is not important for the results.

breakout time. On the other hand, at the opposite end of the distribution of durations, engines active for several hundreds of seconds are required. Long engine durations are invoked also to explain the observed X-ray flares, lasting up to several hours (e.g. Falcone et al. 2007; Lazzati & Perna 2007), although in those cases the evolution of the accretion disk can influence the observed duration (e.g. Perna et al. 2006).

The above considerations highlight the importance that the event duration has for our understanding of the physics of the progenitor star and the immediate aftermath of the explosion. The period of time during which the engine that powers the GRB jet is active is known as  $T_{\text{eng}}$ . The burst's  $T_{90}$  has been generally considered to be a close proxy for its  $T_{\text{eng}}$ , at least after the jet has broken out of the stellar surface (Kobayashi et al. 1997; MacFadyen & Woosley 1999; Bromberg et al. 2011, but see Lazzati et al. 2010). This crucial assumption hence directly relates the observed  $T_{90}$  to the processes in the core of the progenitor star. The aim of this paper is to test the validity of this assumption, and explore various factors that could influence the observed duration of the burst. We achieve this goal by means of two different and complementary analyses. Firstly, we consider a sample of GRBs with well measured redshifts and light curves. We derive the intrinsic light curves and then place them within a redshift range, to examine the  $z$ -dependent variation of the inferred observed duration (instrumental effects and the gamma-ray background playing an important role). Second, and more generally, we generate a large set of synthetic GRB light-power curves from 2D relativistic hydrodynamic simulations of collapsars. We simulate engines of different durations, and explore how the observed GRB  $T_{90}$  varies with viewing angle and redshift of the burst. We are hence able to directly relate the intrinsic length of the GRB engine to what is observed. Last, we create a mock catalogue of GRBs, randomly distributed on the sky with viewing angles, and with a redshift distribution that follows the star formation rate. We explore the effect of different engine durations on the observed GRB distribution, in an attempt to constrain the physical properties of the GRB progenitors.

Our paper is organized as follows. Sect. 2 describes the simulations that we use. The computation of the synthetic lights curves, as well as the properties of the observed and simulated bursts, are described in Sect. 3. We then discuss the results and summarize in Sect. 4. Throughout this paper, we adopt a standard  $\Lambda$ CDM cosmology with  $h_0 = 0.71$ ,  $\Omega_M = 0.27$ , and  $\Omega_\Lambda = 0.73$ .

## 2 NUMERICAL SIMULATIONS

All the simulations presented in this paper were performed with the special-relativistic, adaptive-mesh-refinement hydrodynamic code FLASH, version 2.5 (Fryxell et al. 2000). We adopted a 9 level AMR mesh with a maximum resolution of  $3.9 \times 10^6$  cm at the highest level of refinement. At this resolution the transverse dimension of the injected jet was resolved into at least 46 elements. Our simulations did not include magnetic fields, due to the technical challenge of performing MHD calculations with relativistic motions on an adaptive mesh. In addition, gravity from a central mass and self-gravity were neglected since the characteristic times

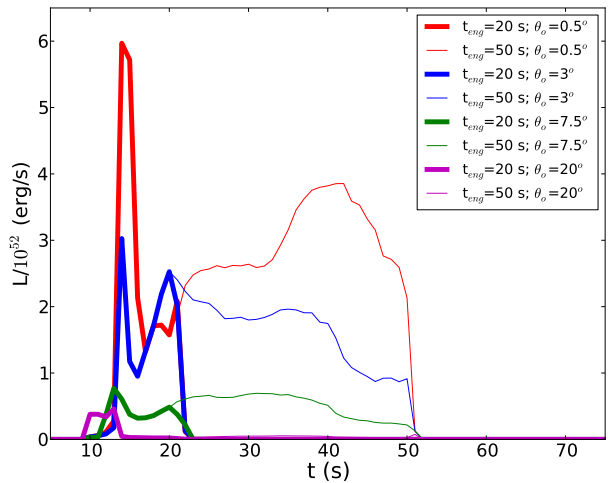


**Figure 1.** Bolometric light-power curves extracted from the simulations with  $T_{\text{eng}} = 20$  and  $50$  s at various off-axis angles. Note how the light-power curves when the engine is active are not affected by the engine duration: the  $20$  s light-power curve coincides with the  $50$  s light-power curve for  $t < 20$  s.

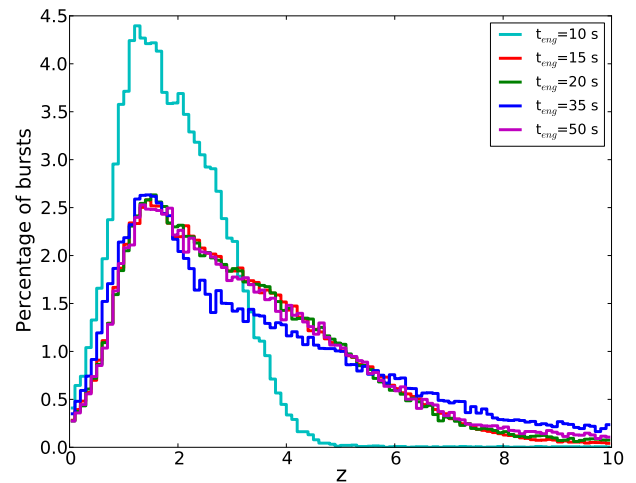


**Figure 2.** Redshift distribution of the detected bursts from the mock catalogues for each of the simulated engines. The vertical axis shows the percentage of bursts falling in each redshift bin.

of the jet-star interaction are much shorter than the dynamical time of the progenitor star's collapse (see, e.g., Lazzati et al. 2012).

All our simulations adopted a realistic GRB stellar progenitor. Specifically, we used model 16TI from Woosley & Heger's (2006) one dimensional pre-SN models. 16TI is a 16 solar-mass Wolf-Rayet star which is rapidly rotating ( $J_0 = 3.3 \times 10^{52}$  erg s), and has low metallicity (1% solar) at the ZAMS. The mass of the star at pre-explosion is 13.95 solar masses and its radius is  $4.07 \times 10^{10}$  cm. The progenitor, which was mapped into a two dimensional domain (assuming cylindrical symmetry), was placed in a constant density

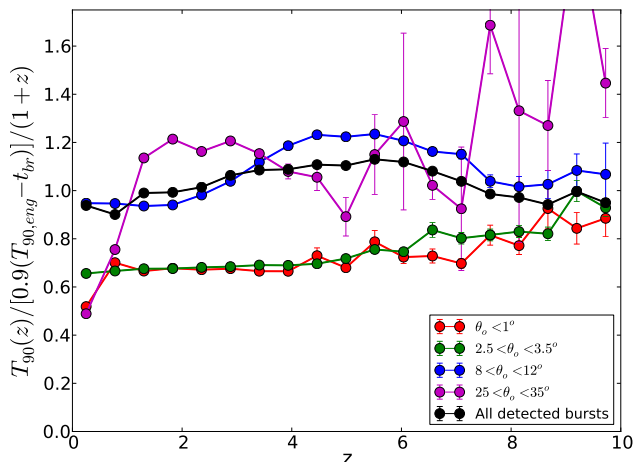


**Figure 3.** Ratio of the duration of the simulated detector light-power curve over the engine 90 percentile duration (after subtracting the breakout time) normalized for cosmological time dilation for the 20 s engine simulation. Different curves show different lines of sight to the observer, as detailed in the legend. Solid lines show the average over many simulations, while error bars, where visible, show the uncertainty associated to the limited size of the simulated sample. All points have an error bar associated with them, but in most cases it is smaller than the marker.

ISM ( $\rho_{ISM} = 10^{-10} \text{ g cm}^{-3}$ ), and had a relativistic jet injected at the inner boundary ( $R_0 = 10^9 \text{ cm}$ ). The jet, with an initial Lorentz factor of  $\Gamma_0 = 5$ , a half-opening angle  $\theta_j = 10^\circ$ , and with enough internal energy to reach an asymptotic Lorentz factor  $\Gamma_\infty = 400$  upon complete non-dissipative acceleration, was injected with a luminosity equal to  $5.33 \times 10^{50} \text{ erg s}^{-1}$  for a certain amount of time (depending on the model). Five different models were used, each with different engine duration ( $T_{\text{eng}}$ ). The durations were 10, 15, 20, 35, and 50 s, after which the jet was turned off for the rest of the 100 s total computation time. The equatorial boundary was set to reflective for the whole duration of the simulation, while the two outer boundaries were set at all times with free outflow conditions. The simulation box was  $2.56 \times 10^{11} \text{ cm}$  in length (along the jet direction) and  $1.28 \times 10^{11} \text{ cm}$  across.

### 3 SYNTHETIC LIGHT CURVES

Light-power curves for the four engine durations were extracted from the 2D simulations following Morsony et al. (2010) for viewing angles between 0.5 and 90 degrees off-axis, assuming 50% radiative efficiency (Figure 1). The figure shows that the light-power curves do not depend on the engine duration while the engine is active. This is not surprising since the engine luminosity is the same for every simulation, and the jet head is not in causal connection with its base. If we had chosen to keep the total ejected energy constant and made the shorter engines more luminous, the light curves from short and long engines would not have overlapped, even at the

early times when both engines are active. Bolometric light-power curves were converted into observed countrates as:

$$\Phi = B + \frac{AL_{\text{bol}}}{4\pi d_L^2} \int_{\epsilon_m}^{\epsilon_M} \frac{B_{\alpha,\beta,E_0/(1+z)}(\epsilon)}{1.6 \times 10^{-9} \epsilon} d\epsilon, \quad (1)$$

where  $\Phi$  is in counts per second,  $B$  is the background in counts per second,  $A$  is the effective area of the adopted instrument in  $\text{cm}^2$ ,  $\epsilon_m$  and  $\epsilon_M$  are the lower and upper sensitivity bounds of the adopted instrument in keV, respectively,  $L_{\text{bol}}$  is the bolometric luminosity in erg/s,  $d_L$  is the luminosity distance in cm,  $\epsilon$  is the photon energy in keV, and  $B_{\alpha,\beta,E_0}(\epsilon)$  is a normalized Band function (Band 1983) with low-frequency slope  $\alpha$ , high-frequency slope  $\beta$ , and peak frequency  $E_0$ . The Band function is normalized so that:

$$\int_0^\infty B_{\alpha,\beta,E_0}(\epsilon) d\epsilon = 1 \quad (2)$$

In order to mimic GRBs detected by BATSE, we assumed  $B = 10000$ ,  $[\epsilon_m, \epsilon_M] = [25, 2000] \text{ keV}$ , and  $A = 2000 \text{ cm}^2$ . Average values for the spectral slopes  $\alpha = 0$  and  $\beta = -1.5$  were also assumed<sup>2</sup>. Finally, the peak frequency  $E_0$  was set to follow the intra-burst luminosity-peak-frequency correlation and obey (Ghirlanda et al 2010; Lu et al 2012):

$$E_0 = 10^{0.53 \log_{10}(L_{\text{bol}}) - 25.3}. \quad (3)$$

Mock GRB catalogs were constructed for each engine duration by exploding massive stars at a rate proportional to star formation<sup>3</sup> SFR2 in Porciani & Madau (2001). SFR2 assumes that the comoving star formation rate is flat at high redshift. The exploding stars were randomly oriented with respect to the line of sight and a detection algorithm was applied to the resulting synthetic countrate curves. Countrate curves that produced a  $5\text{-}\sigma$  increase in the countrate on at least one timescale among 1, 5, and 25 seconds were labeled as “detections”. Figure 2 shows the redshift distribution of the detected busts for the five different engine durations.

Figure 3 shows the redshift dependence of the ratio of the  $T_{90}(z)$  measured from the synthetic light-power curves over the expected duration expressed as  $0.9(T_{\text{eng}} - T_{\text{br}})$ , i.e., 90% of the time interval during which the engine energy is released minus the breakout time. In our simulations the engine had constant luminosity and  $T_{\text{bo}}$  was measured to be  $\sim 8 \text{ s}$ . The curves were also divided by  $(1+z)$  to remove the cosmological dilation and enhance the role of spectral evolution on the measurement of the duration of the light curve. The figure shows results for the  $T_{\text{eng}} = 20 \text{ s}$  simulation, but results from the other simulations are similar, except for the  $T_{\text{eng}} = 10 \text{ s}$  simulation, where very few bursts are detected at large redshifts, even for small viewing angle (see Figure 2). This

<sup>2</sup> Note that we here define  $\alpha$  and  $\beta$  as the spectral indices, not the photon indices.

<sup>3</sup> We note that the assumption that the GRB rate strictly follows the star formation rate is highly debated in the literature. Several studies (e.g. Wanderman & Piran 2010) suggest that the relative GRB-to-star formation rate is higher at higher redshift, although observational biases might contribute to this effect (e.g. Kistler et al. 2009; Robertson & Ellis 2012; Trenti et al. 2012).

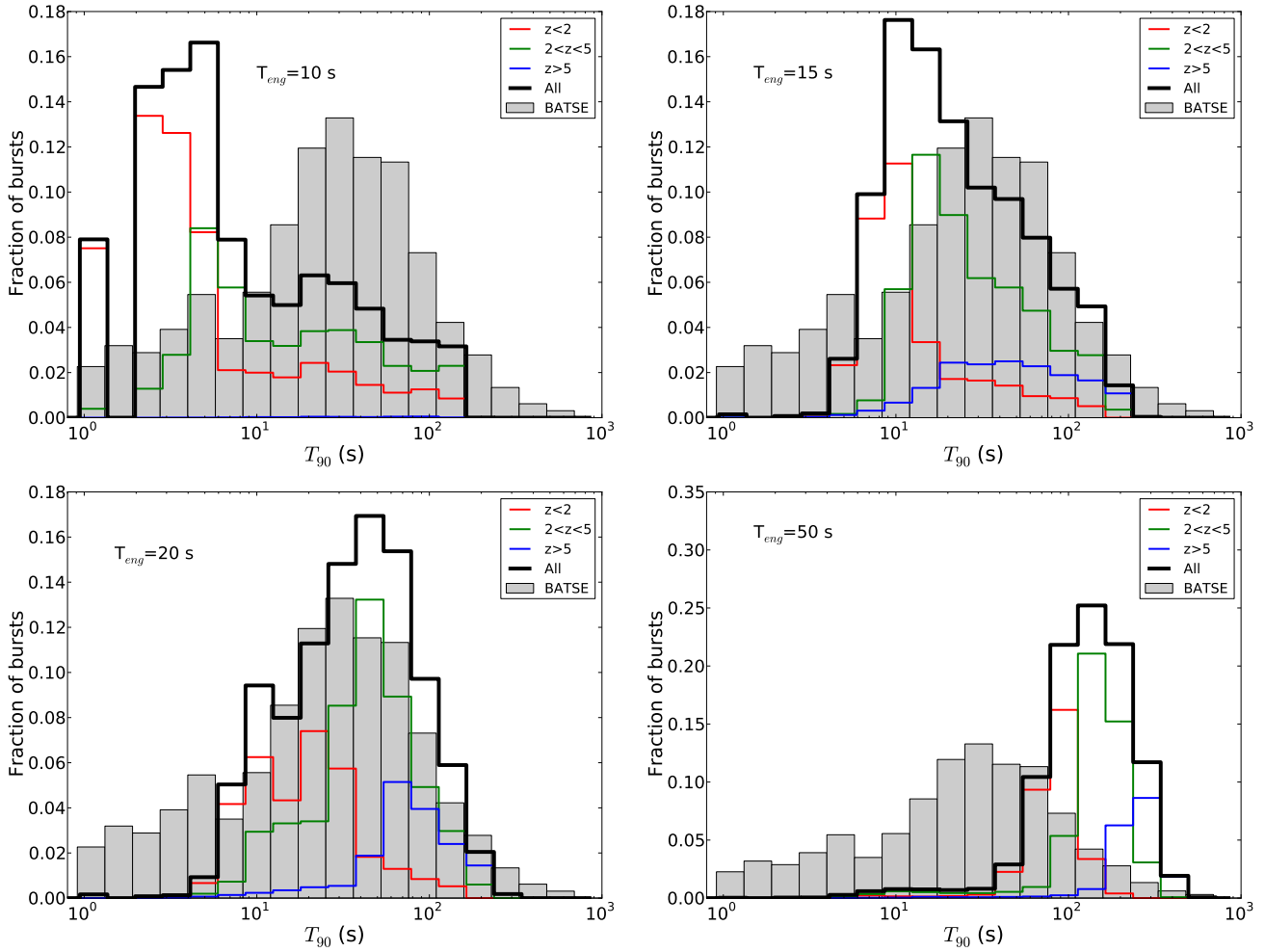


**Figure 5.** Distribution of the BATSE duration catalog (shaded histogram) and of the mock catalogs generated from simulations with  $T_{\text{eng}} = 15$  s (upper left panel), 20 s (upper right panel), 35 s (lower left panel), and 50 s (lower right panel). In all panels, the thick solid line is the duration distribution of the whole mock catalog, while the colored lines show the partial distribution in selected redshift bins.

seems to be due to the fact that these shorter bursts have lower fluence and are not detectable in the longer time-scale of 25 seconds.

Figure 3 illustrates two important findings: first, the observed light-power curve duration is on average a good proxy for the engine duration, if the breakout time is subtracted. However, the  $T_{90}$  can be much shorter than the engine duration, especially for bright, on-axis, low-redshift events. This is partly due to the fact that hydrodynamic collimation makes the jet opening angle a time-dependent quantity, causing some observers to see only very dim emission when the jet angle is smaller than their viewing angle. Indeed, the  $T_{90}$  duration measured from the light curve has a marked dependence on the viewing angle, the on-axis bursts lasting less the off-axis ones for the same jet-progenitor pair. Second, there is only modest evolution of the observed  $T_{90}$  with redshift, once the dominant  $(1+z)$  component is removed. The figure suggests a moderate increase of the duration with redshift for on-axis observers,

a decrease for wide-angle observers, and a mixed behavior for observers at intermediate angles. At large redshifts, only a few of the simulated curves are detected, and the measured duration is dominated by the statistical error, creating the impression of a growth of the duration with redshift which is instead due to the fact that the burst is so faint that large chunks of background are mistakenly included in the  $T_{90}$  measurement. This inaccuracy is intrinsic to non-imaging counting instruments like BATSE, and we haven't therefore applied any correction since we are comparing to BATSE results. In the same figure, a black line shows the average  $T_{90}$  observed as a function of redshift for the detected bursts. The black line takes into account the fact that there are less small viewing angle bursts and that large viewing angle bursts are intrinsically faint and hard to detect. For these reasons, it mimics fairly closely the intermediate viewing angle line.

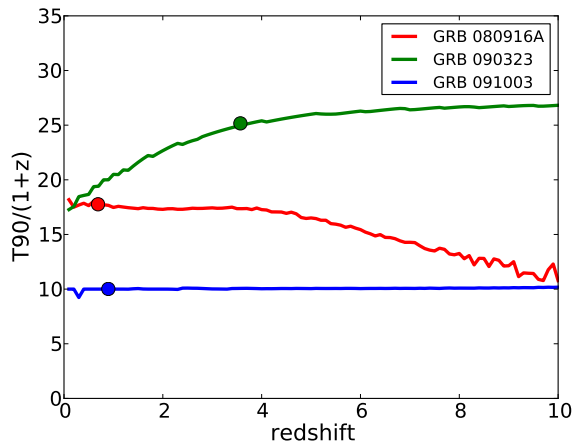


**Figure 4.** Detected duration of selected Fermi GRBs as a function of hypothetical redshift. A solid symbol shows, for each burst, the redshift and duration with which it was actually detected.

GRB	$z$	$E_{pk}[keV]$	Fluence[erg/cm <sup>2</sup> ]
080916A	0.689	107.41	7.81e-6
090323	3.5774	639.31	1.18e-4
091003	0.8969	366.44	2.33e-5

**Table 1.** Properties of the observed GRBs used for computing the redshift evolution of their observed  $T_{90}$  duration.

In order to compare the results of Figure 3 with observations, we selected three GRBs observed by Fermi in a wide spectral range for which extensive time-dependent spectral analysis has been performed (Lu et al. 2012). These are GRB 080916A, GRB 090323, and GRB 091003, whose general properties ( $\alpha$ ,  $\beta$ ,  $E_{pk}$  and flux, from Lu et al. 2012) are reported in Table 1. Then, Eq. 1 was used to convert such properties into simulated light-power curves for the same burst as they would have been observed from different redshifts. The results of these calculations are seen in Figure 4. As for the simulated light-power curves, we see that there is only a moderate evolution with redshift, once the effect of cosmological time dilation has been removed. One burst has a constant observed  $T_{90}$ , one has a growing one, and one has a decreasing one. The different behavior is connected to the peak frequency of the emission. Softer bursts are consistently redshifted out of the instrument band and become therefore shorter with redshift. Harder bursts are instead redshifted into the instrument band and become longer with redshift.

A final comparison can be performed between the BATSE  $T_{90}$  distribution and the distribution of the  $T_{90}$  of the simulated bursts from the mock catalogs. Each panel in Figure 5 shows the comparison for a different engine duration. The BATSE distribution is always shown with a shaded histogram, while the mock distribution

is shown with a thick solid line. For the mock catalogs only, the distribution of durations from bursts in selected redshift bins is shown with colored lines. The comparison shows that most of the width of the duration distribution can be accounted for by a single progenitor star and engine duration combination. Several effects contribute in broadening the duration distribution from a single progenitor. First, the redshift time-dilation systematically increases the observed duration of distant bursts. Second, the uncertainty associated with the difficulty of selecting the starting and ending point of a weak GRB overlaid on a noisy background can affect both positively and negatively the duration of a burst, especially if observed at wide angle and/or at high redshift. This effect is the main contributor to the population of bursts with detected durations much shorter than the engine duration. Finally, the dependence of the observed duration on the viewing angle can moderately decrease the observed duration (up to a factor  $\sim 2$  for the brightest bursts). To quantify this statement, we show in Figure 6 the result of fitting the BATSE distribution with a linear combination of the distributions from the five mock catalogs. The BATSE distribution was purged of any bursts with  $T_{90} < 1$  s in order to eliminate short-duration GRBs that cannot be accounted for in this model. The fit was performed by minimizing the  $\chi^2$  allowing for the BATSE detected burst to have free contributions from the various engine durations (each population percentage being allowed to vary independently between 0 and 100 and constraining the sum of all percentages to be equal to 100). We find that the overall shape of the BATSE duration distribution can be accounted for by an engine duration distribution strongly peaked at  $T_{eng} = 20$  s (70% of the bursts) with a small component of shorter engines (21% with  $T_{eng} = 10$  s and 4% with  $T_{eng} = 15$  s) and a minor component of longer engines (5% with  $T_{eng} = 50$  s). No engine with  $T_{eng} = 35$  s is required to fit the BATSE distribution.

## 4 DISCUSSION AND CONCLUSIONS

We have used numerical simulations to investigate the connection between the intrinsic engine duration and the light curve duration in long GRBs and the origin of the observed duration distribution. Our main conclusions and a discussion of their caveats, limitations, and implications are:

(i) The observed light curve duration of the prompt emission of GRBs is, on average, a good proxy for the engine duration, after subtracting the jet breakout time. However, our study reveals a dependence of the burst duration on the viewing angle especially for burst at low redshift observed very close to the jet axis. The same progenitor and engine pair can therefore produce somewhat different bursts, those observed on-axis being brighter and shorter and those observed at an off-axis angle being longer and fainter.

(ii) The duration of the same event hypothetically seen at different redshifts is fairly constant, once the effect of cosmological time dilation is accounted for, in both simulated and observed bursts. In this regard it is important to point out that our simulated engines had constant luminosity until they were suddenly shut-off. Engines with smoothly decaying tails could produce bursts with long-lasting

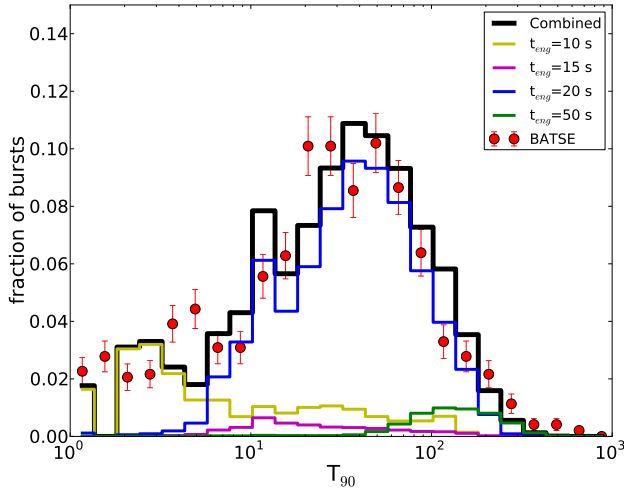


**Figure 6.** Fit of the BATSE duration distribution of long GRBs with a linear combination of the mock catalogs for different engine durations.

X-ray tails that may produce a stronger effect when viewed at different redshifts. In the case of observed light curves, our method could have missed X-ray tails as well, since we relied on the possibility of performing spectral analysis of the observed light curves and therefore of a minimum number of photon counts. Soft, weak, long-lasting X-ray tails would have been missed in the observations as well as in the simulations. The consistent qualitative behavior between simulated and observed light curves should therefore be seen more as an indication that they were analyzed consistently rather than as a strong evidence of the lack of a redshift-dependent duration evolution.

(iii) Assuming a flat star formation rate at high-redshift, most of the BATSE duration distributions of long GRBs can be accounted for with only a very small range of engine durations (between 10 and 20 s). Only a very small fraction of very long-lasting engines are required to explain the long duration tail and, possibly, the recently-detected population of very long bursts (Gendre et al. 2013; Levan et al. 2013). The width of the BATSE duration distribution is almost entirely accounted for by the effect of the viewing angle and of the broad range of redshift at which bursts can be detected. The observed burst population is therefore dominated by engines with a duration significantly smaller than what has been explored numerically (e.g. Lazzati et al. 2010, 2013). We show instead with this study that the typical engine duration of a burst from a compact Wolf-Rayet star is  $\sim 20$  s.

## ACKNOWLEDGEMENTS

We thank S.E. Woosley and A. Heger for making their pre-SN models available. The software used in this work was in part developed by the DOE-supported ASC/Alliance Center for Astrophysical Thermonuclear Flashes at the University of Chicago. MV acknowledges support from NSF grant AST-1062736 for her participation in the URCA summer program at NCSU, where this work was

initially developed, and the Undergraduate Research Opportunities Program at the University of Colorado Boulder. This work was supported in part by the Fermi GI program grants NNX10AP55G and NNX12AO74G (DL & DLC), and by NSF Grant No. AST 1009396 (RP). BJM is supported by an NSF Astronomy and Astrophysics Postdoctoral Fellowship under award AST-1102796.

## REFERENCES

- Aloy M. A., Müller E., Ibáñez J. M., Martí J. M., MacFadyen A., 2000, *ApJ*, 531, L119
- Bromberg O., Nakar E., Piran T., Sari R., 2011, *ApJ*, 740, 100
- Bromberg O., Nakar E., Piran T., Sari R., 2013, *ApJ*, 764, 179
- Bucciantini N., Quataert E., Metzger B. D., Thompson T. A., Arons J., Del Zanna L., 2009, *MNRAS*, 396, 2038
- Falcone A. D., et al., 2007, *ApJ*, 671, 1921
- Fryxell B., et al., 2000, *ApJS*, 131, 273
- Gehrels N., et al., 2006, *Natur*, 444, 1044
- Gendre B., et al., 2013, *ApJ*, 766, 30
- Ghirlanda G., Nava L., Ghisellini G., 2010, *A&A*, 511, A43
- Kistler M. D., Yüksel H., Beacom J. F., Hopkins A. M., Wyithe J. S. B., 2009, *ApJ*, 705, L104
- Kobayashi S., Piran T., Sari R., 1997, *ApJ*, 490, 92
- Kouveliotou C., Meegan C. A., Fishman G. J., Bhat N. P., Briggs M. S., Koshut T. M., Paciesas W. S., Pendleton G. N., 1993, *ApJ*, 413, L101
- Lazzati D., Perna R., 2007, *MNRAS*, 375, L46
- Lazzati D., Morsony B. J., Begelman M. C., 2010, *ApJ*, 717, 239
- Lazzati D., Morsony B. J., Blackwell C. H., Begelman M. C., 2012, *ApJ*, 750, 68
- Lazzati D., Morsony B. J., Margutti R., Begelman M. C., 2013, *ApJ*, 765, 103
- Levan A. J., et al., 2013, *ApJ* submitted, arXiv:1302.2352
- López-Cámara D., Morsony B. J., Begelman M. C., Lazzati D., 2013, *ApJ*, 767, 19
- Lu R.-J., Wei J.-J., Liang E.-W., Zhang B.-B., Lü H.-J., Lü L.-Z., Lei W.-H., Zhang B., 2012, *ApJ*, 756, 112
- MacFadyen A. I., Woosley S. E., 1999, *ApJ*, 524, 262
- Morsony B. J., Lazzati D., Begelman M. C., 2007, *ApJ*, 665, 569
- Morsony B. J., Lazzati D., Begelman M. C., 2010, *ApJ*, 723, 267
- Nagataki S., 2011, *PASJ*, 63, 1243
- Nakar E., 2007, *PhR*, 442, 166
- Perna R., Armitage P. J., Zhang B., 2006, *ApJ*, 636, L29
- Porciani C., Madau P., 2001, *ApJ*, 548, 522
- Robertson B. E., Ellis R. S., 2012, *ApJ*, 744, 95
- Trenti M., Perna R., Levesque E. M., Shull J. M., Stocke J. T., 2012, *ApJ*, 749, L38
- Usov V. V., 1992, *Nature*, 357, 472
- Wanderman D., Piran T., 2010, *MNRAS*, 406, 1944
- Woosley S. E., Bloom J. S., 2006, *ARA&A*, 44, 507
- Woosley S. E., Heger A., 2006, *ApJ*, 637, 914
- Zhang W., Woosley S. E., MacFadyen A. I., 2003, *ApJ*, 586, 356
- Zhang B., Zhang B.-B., Liang E.-W., Gehrels N., Burrows D. N., Mészáros P., 2007, *ApJ*, 655, L25